AIAA AVIATION Forum
June 15-19, 2020, VIRTUAL EVENT
AIAA AVIATION 2020 FORUM

10.2514/6.2020-3237

PSP Studies of the Wake Response Downstream of a Spanwise-Oscillating Hemispherical Turret

Aaron Roeder[1], Daiki Kurihara[2] , Hirotaka Sakaue[3], Stanislav Gordeyev[4],
University of Notre Dame, Notre Dame, IN, 46556

The wake response downstream of a spanwise-oscillating hemispherical turret was investigated experimentally using Pressure Sensitive Paint (PSP), along with several unsteady pressure sensors, placed on the turret and on the tunnel wall. PSP was painted on the turret and in the wake region in order to compare the globally reconstructed pressure fields between oscillating and stationary cases. It was found that pressure fluctuations were less energetic for the oscillating turret and the wake was more organized in the spanwise direction, compared to the stationary turret wake. POD and DMD analysis of the reconstructed pressure fields revealed the wake is characterized by global shifting and breathing wake modes, and it was confirmed that the wake dynamics were suppressed when the flow forced the turret to oscillate at a predominantly single frequency. The suppressive effects of the turret oscillations on the wake dynamics were found to become more robust at higher freestream Mach numbers, and the normalized wake response frequency was found to be higher than the normalized resonant frequency of turret oscillations.

I. Introduction

Hemispherical turrets provide an optimal geometry for maximizing field-of-regard for laser tracking systems used in airborne applications. However, when aircraft are instrumented with turret-based systems, turbulent flow around the turret and throughout the wake characterized by sharp density gradients induces variations in fluctuating index-of-refraction due to the protruding nature of the turret. Laser light propagated through regions of air containing spatio-temporal variability in index-of-refraction will aberrate the incident beam. Thus, the ramifications of aero-optical distortions on hemispherical turrets as beam directors are significant in their effectiveness to potentially degrade the point-and-track capabilities of Adaptive-Optics systems.

Both spanwise and streamwise surface curvature characterize hemispherical turret systems, leading to flow separation on top of the turret at high transonic speeds, along with a complicated three-dimensional flow field in the wake resulting from horn vortices caused by the flow separation and necklace vortices created from boundary layer interactions with the turret leading edge. Additionally, unsteady forces acting on the turret from the turbulent flow field could potentially

[1] Graduate Student, Department of Aerospace and Mech. Eng., AIAA Student Member.
[2] Graduate Student, Department of Aerospace and Mech. Eng., AIAA Student Member.
[3] Associate Professor, Department of Aerospace and Mech. Eng., AIAA Senior Member
[4] Associate Professor, Department of Aerospace and Mech. Eng., AIAA Associate Fellow

excite unwanted mechanical vibrations inside the delicate optical layout of the turret, which adversely affects beam control system performance.

These effects have been widely studied in order to quantitatively analyze the aero-optical [1-5] and fluid-dynamical [6-11] effects of turrets. Pressure sensitive paint studies have been conducted in order to reconstruct the spatially-resolved unsteady global pressure field on and around turrets at both subsonic and transonic flow regimes [12-15], and more recent studies have found that the dynamics of the wake is primarily characterized by a shifting mode, characterized by the dominant frequency $St_D = 0.1\text{-}0.15$ using a conditional analysis of the global pressure field on and around the turret along with proper orthogonal decomposition (POD) as described in [14,15,16].

All aforementioned studies have assumed that the motion of the turret system relative to the airborne platform is negligible. However, if the turret is not rigidly mounted or the turret skin is thin in order to minimize the overall mass of the turret assembly, unsteady forces resulting from unsteady pressure fields can induce mechanical motion or possibly elastic deformation of the turret itself. Such changes could cause substantial deviations in the wake behavior from previously understood results that, in turn, would affect the unsteady forces acting on the turret.

In the presented studies, a 10 in. diameter hemispherical turret was allowed to oscillate solely in the spanwise direction by mounting it on a flexible cantilever beam. The oscillating turret system was designed and built such that the dominant vibrational frequency matches the dominant frequency of the unsteady spanwise forcing of the flow on the turret, in order to utilize resonance-related oscillation amplitude amplification. An alternate configuration allowed the turret to be rigidly affixed with respect to the oscillating case, and it was previously confirmed in [17] that this arrangement adequately restricted the spanwise motion of the turret.

The turret and wake region were both painted with fast-response, porous, pressure sensitive paint (PSP) in order to compare the globally-reconstructed flow fields between the oscillating and stationary cases. PSP contains molecules called luminophore that are sensitive to oxygen and fluoresce when the molecules are exposed to ultraviolet light. As the pressure inside the tunnel decreases, the concentration of oxygen in the air decreases proportionally, causing the paint to glow. Higher concentrations of oxygen quench the luminescence of the paint, so the painted regions on the model which experience lower pressure will glow more brightly than regions which experience higher pressure. New technological advancements in recent years has allowed the response time of PSP to decrease significantly.

II. Experimental Studies

The oscillating turret design consisted of a plastic 10” diameter hemispherical dome mounted on a thin rectangular aluminum plate of 0.5” thickness that was allowed to freely vibrate solely in the spanwise direction. A schematic of the oscillating turret design is presented in Figure 1, left. The length of the aluminum plate was chosen in such a way that the turret/plate assembly would behave as a cantilever beam with an added mass, with a resonant frequency of 90 Hz, which would coincide with the dominant frequency range of the spanwise forcing, $St_D \sim 0.15$, acting on the turret, see [17] for details of the turret assembly design and dynamic analysis. To allow for the turret motion, the bottom of the mounting plate with the hemisphere on it was aligned with the tunnel wall with a small gap in between on the order of a millimeter. The oscillating turret system was converted to a stationary turret configuration by inserting metal spacers between the mounting plate and the underside of the turret, where the metal spacers physically wedged the turret and plate against the tunnel wall, allowing the motion of the turret system to be coupled with the wall. These configurations enabled two different sets of experiments to be conducted in order for the wake flow physics and dynamic effects of the oscillating turret to be compared to the same, but stationary turret.

Both the oscillating and stationary turret configurations were tested in the University of Notre Dame White Field 3' x 3' wind tunnel facilities over a range of freestream Mach numbers between M = 0.30 and M = 0.60. A summary of the conditions for both tests is presented in Table 1. Four 400 nm ultraviolet lights (ISSA LM2-400 type) were used to illuminate the PSP on and around the turret, as shown in Figure 2. A very thin uniform layer, < 1mm, of PSP was sprayed on the plastic dome and the surrounding aluminum mounting wall section before testing was conducted. The binder material was polymer-ceramic PSP (PC-PSP), which consisted of Silicone RTV as the polymer and bathophen ruthenium as the luminophore. Two high-speed cameras, Phantom v1611 and Phantom v2512, were used to record the intensity fluctuations emitted by the PSP. Both cameras were run at a sampling frequency of 3 kHz at the maximum pixel resolution of 1280 x 800. The v1611 camera collected 16541 frames over 5.51 seconds, and the newer v2512 camera collected 49685 frames over 16.56 seconds. Seven Kulite differential pressure transducers were used for in-situ calibration of the PSP; four Kulites were installed on the turret model and three Kulites were instrumented in the wake. A photograph of the painted and installed turret along with the exact locations of the Kulites are shown in Figure 1, right. Independent calibration curves for each Kulite were constructed using a pressure chamber before the Kulite were instrumented. The Kulites were sampled at 30 kHz for 30 seconds.

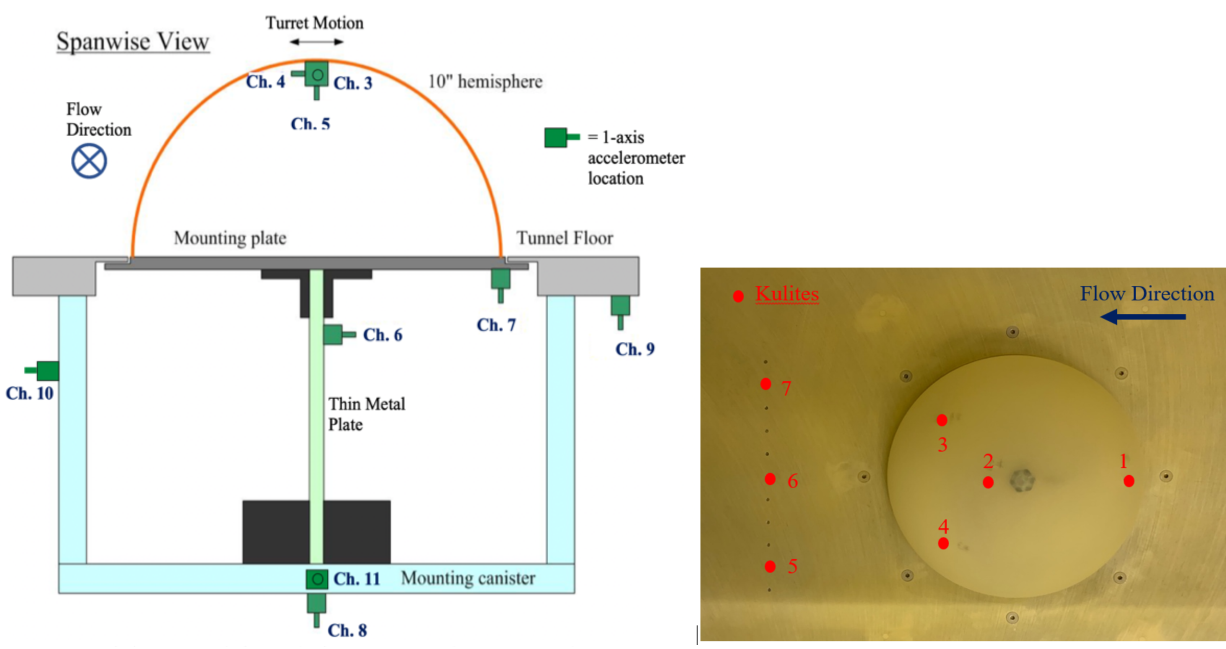

Figure 1: Schematic of the oscillating turret with accelerometer locations (left), and photo of installed turret and wake painted with fast-response PSP with Kulite locations in red (right).

Table 1: Properties and run conditions of the turret configurations.

Configuration:	Incoming Mach Numbers:	Camera Sampling Frequency:	Kulite Sampling Frequency	Accelerometer Sampling Frequency	Sampling Time:
Oscillating	0.30, 0.40, 0.50, 0.60	3 kHz	30 kHz	3 kHz	30 s
Stationary	0.30, 0.40, 0.50, 0.60	3 kHz	30 kHz	3 kHz	30 s

To study the turret motion, a total of eight 1-axis accelerometers were affixed to various locations inside of the turret and on the mounting plate and mounting canister, as shown in Figure 1, right. The accelerometers were sampled at 30 kHz for 30 seconds. Triggering of the accelerometers was synchronized with both high-speed cameras using the falling edge of a single square pulse from Keysight 33500B Waveform Generator with a 100-mV peak-to-peak pulse amplitude and 1-mV pulse width.

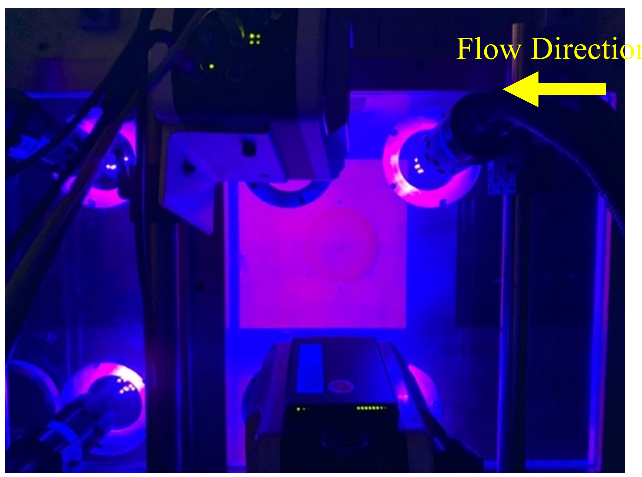

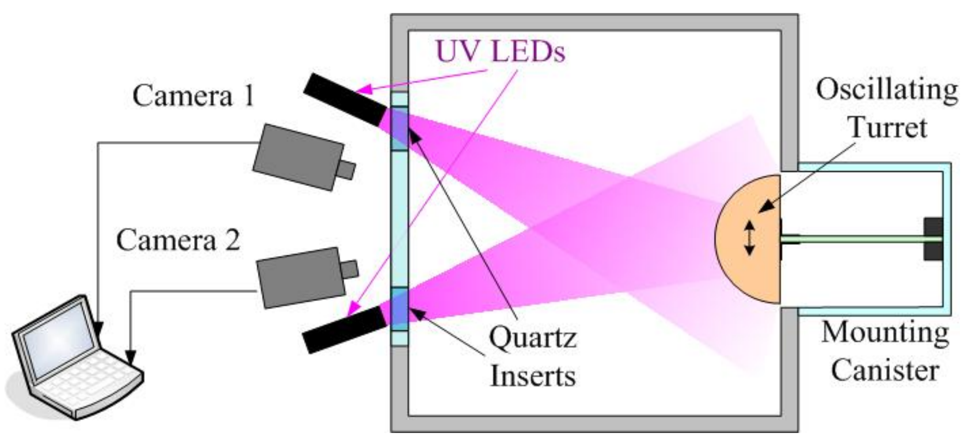

Figure 2: Top: Painted and installed turret and wake under 400 nm illumination from four UV light sources along with positions of Phantom v1610 (Camera 1) and Phantom v2512 (Camera 2) high-speed cameras. Bottom: Schematic of the experiments.

III. Data Analysis

Pressure spectra from PSP intensity data around Kulite 6, located in the middle of the wake, was extracted and is compared to the Kulite spectra in Figure 3. The agreement between the spectra is reasonable, and the paint was found to correctly resolve the unsteady pressure spectrum up to approximately 50% of the Nyquist frequency of 1,500 Hz. A similar agreement was found using the PSP at the other six Kulite locations, verifying the accuracy of the in-situ calibration. The slight deviations at higher frequencies are attributed as a characteristic of the PSP response.

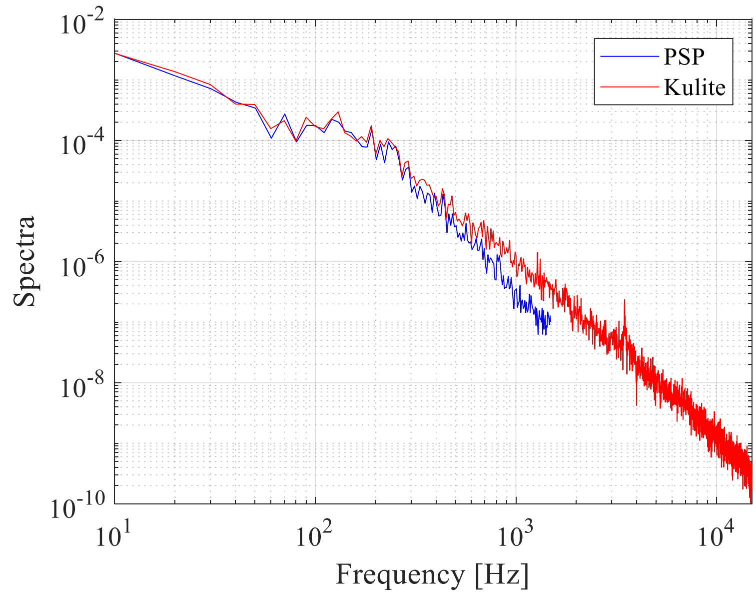

Figure 3: Comparison of normalized PSP pressure spectra for the oscillating turret at M = 0.5 with Kulite 6 spectra (see Figure 1, right) in the middle of the wake.

The instantaneous intensity variations, I, emitted by the PSP are related to the instantaneous pressure fluctuations, P, via the Stern-Volmer equation, as given by equation (1),

$$\frac{I_{ref}}{I} = A + B\frac{P}{P_{ref}} \tag{1}$$

where I_{ref} and P_{ref} describe the instantaneous intensity and pressure fluctuations, respectively, under a set of reference conditions, and A and B are experimentally determined constants. Reference data was collected before each test under no flow conditions with the ultraviolet lights turned on and illuminating the PSP. The average intensity from PSP in the region immediately surrounding each of the seven Kulites was extracted and computed under the reference conditions and at each of the four Mach numbers tested, and the static pressure from the Kulites were used in order to determine A = 0.64 and B = 0.33. The calibration curve from the in-situ calibration is presented in Figure 4.

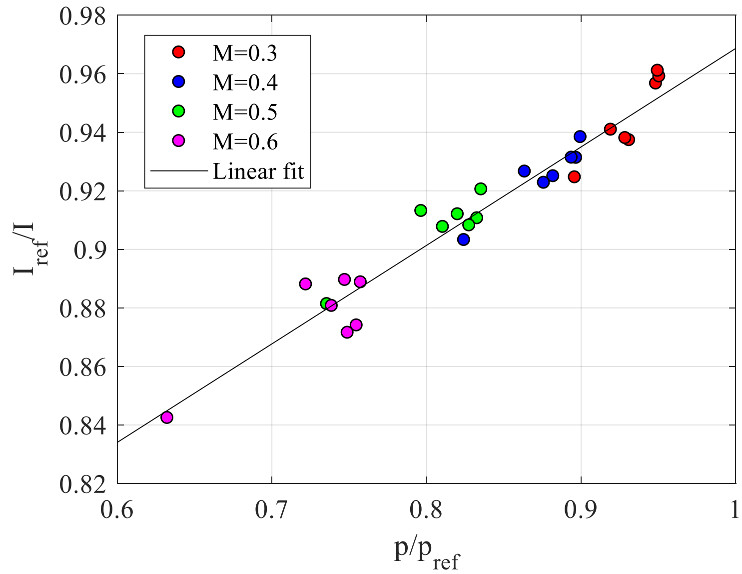

Figure 4: Calibration curve using in-situ PSP data for M = 0.3 – 0.6.

Joint Proper Orthogonal Decomposition (JPOD) was employed as a data analysis technique to compute the common modes from the pressure fields in the wake region downstream of the oscillating and stationary turret configurations for all tested Mach numbers [12]. In POD, the globally-reconstructed spatiotemporal pressure field, $p(s,t)$, is decomposed into a series of N orthogonal spatial modes, $\varphi(s)$, and corresponding temporal coefficients, $a_k(t)$, given by equation (2) [12].

$$p(s,t) = \sum_{n=1}^{N} \varphi_n(s) a_n(t) \tag{2}$$

POD is commonly used as a means for creating a low-order reconstruction of the pressure field, where the total unsteady pressure energy in the field can be adequately represented using a reduced number of modes. Although an optimal set of eigenmodes can be obtained for each data set using POD, the sets are different for each case, so comparing different cases becomes very complicated. JPOD is a specialized version of POD in which the spatio-temporal pressure fields for different cases are combined into a single joint pressure field, $p_{joint}(s,t)$, in order to produce the spatial modes, which are common to all cases, as given by equation (3),

$$p_{joint}(s,t) = \{p(s,t,\Lambda_1), p(s,t,\Lambda_2), \cdots\} \tag{3}$$

where Λ is some unique parameter which characterizes each case. The corresponding joint correlation matrix, R_J, is given by the average of all of the individual correlation matrices, as presented in equation (4) [12].

$$R_J(s,s') \equiv \frac{1}{N} \sum_{All\ \Lambda}^{N} R(s,s';\Lambda) \tag{4}$$

The temporal coefficients, a_n, and corresponding eigenvalues, λ_n, for the JPOD modes are found using equations (5) and (6), respectively, where φ_n are the spatial modes common to both parameters, Λ, and double integration denotes a surface integral [12].

$$a_n(t;\Lambda) = \iint p(s,t;\Lambda)\varphi_n(s)ds \tag{5}$$

$$\lambda_n(\Lambda) = \overline{a_n^2(t;\Lambda)} \tag{6}$$

The JPOD spatial modes are computed as the eigenvectors of the joint correlation matrix, R_J. The modes produced using JPOD are ordered in terms of energy content, where the first mode contains the most energy. In this analysis, the pressure fields are characterized by only two parameters, representative of the oscillating and stationary turret configurations. The unsteady pressure fields for each case were projected onto the JPOD modes in order to extract the temporal evolution of the modes. Since the modes are the same for both cases, the differences in the wake dynamics are reflected in the temporal coefficients only, along with the individual and cumulative mode energies.

In order to further investigate the wake response due to flow-induced oscillations of the hemispherical turret, Dynamic Mode Decomposition (DMD) was used to analyze the dynamics and topology of the globally-reconstructed spatio-temporal pressure fields from PSP. DMD decomposes a pressure field into a series of spatial modes, $\psi_k(s)$, eigenvalues, λ_k, and amplitudes, c_k, which correspond to each eigenvalue. DMD modes are computed as a function of frequency, where each DMD mode corresponds to a given fixed frequency. The algorithm used to compute DMD modes using the standard method is fully discussed in [19]. The formula for the DMD decomposition of a given pressure field, p(s,t), is given by equation (7).

$$p(s,t) = \sum_k c_k e^{\lambda_k t}\phi_k(s) \tag{7}$$

The discrete Fourier transform (DFT) method of DMD was used to actually compute DMD modes from the wake PSP pressure fields. The simplified version of DMD which uses the mean-removed data set is presented in full detail in [21]. The DMD modes for the mean-removed dataset are simply given by the DFT of the full dataset in time, so performing the analysis using the DFT method saved a significant amount of computational cost with respect to the standard DMD method. The DMD amplitudes are found using equation (8),

$$c_k^2 = \sum_{m=1}^{M} \tilde{\phi}_k^*(\vec{x}_m)\tilde{\phi}_k(\vec{x}_m) \tag{8}$$

where $\tilde{\phi}_k$ is the set of non-normalized spatial modes given by equation (9).

$$\tilde{\phi}_k(\vec{x}) = \frac{1}{N+1}\sum_{j=0}^{N} p(\vec{x},t)e^{-2\pi i\frac{k\cdot j}{N}}, \qquad k = 1 \dots N \tag{9}$$

The DMD spatial modes are then normalized by the amplitudes, as given by equation (10).

$$\phi_k(\vec{x}_m) = \tilde{\phi}_k(\vec{x}_m)/c_k \tag{10}$$

The unsteady pressure fields from PSP were mapped onto the turret itself using a 3D Perspective Transformation Matrix and a non-uniform rectangular grid. The unsteady force, $\vec{F}$, on the turret was computed using equation (11),

$$\vec{F}(x,y,z,t) = \oint (p(x,y,z,t) * \vec{n}\,(x,y,z)) \cdot dS \tag{11}$$

where $\vec{n}$ are the normal vectors on the turret and dS represents the surface area of a single grid element for the hemisphere with total surface area, S. Equation (11) was actually implemented by multiplying the pressure field over the whole turret by the normal vectors and the surface areas of the non-uniform grid for each time step, and then summing the resulting quantity over all time steps in order to obtain the unsteady forces in all three dimensions. The surface areas of the elements of the non-uniform grid served as spatial weighting functions for integrating the pressure fields.

IV. Results

In order to confirm that the turret did oscillate at the designed resonant frequency of 90 Hz and the spanwise motion of the stationary configuration was restricted with respect to the oscillating case, power spectral density from the accelerometer positioned in the spanwise direction on the turret model was computed for both cases and compared with results from previous tests. These results are presented in Figure 4, where M = 0.45 was the highest freestream Mach number achieved in the 2018 set of tests [17]. The resonant frequency of the oscillating turret was measured to be approximately 84 Hz, which agrees reasonably well with previous findings and the overall shapes and magnitudes of both vibrating and stationary sets of spectra adequately concur across all sampling frequencies. The amplitude of the resonant peak is more than 25 times larger than the largest peaks for the stationary turret. Additionally, a first harmonic peak with smaller amplitude at 178 Hz is also present in the oscillating turret spectra, which indicates a presence of non-linear effects in the turret response. The accelerometer spectra of the spanwise motion of the oscillating turret was also determined to be less correlated with the wind tunnel wall vibrations compared to the stationary case, indicating that the turret vibrations are induced solely by the flow and the design of the cantilever system, which can be modeled using Euler-Bernoulli beam theory [18].

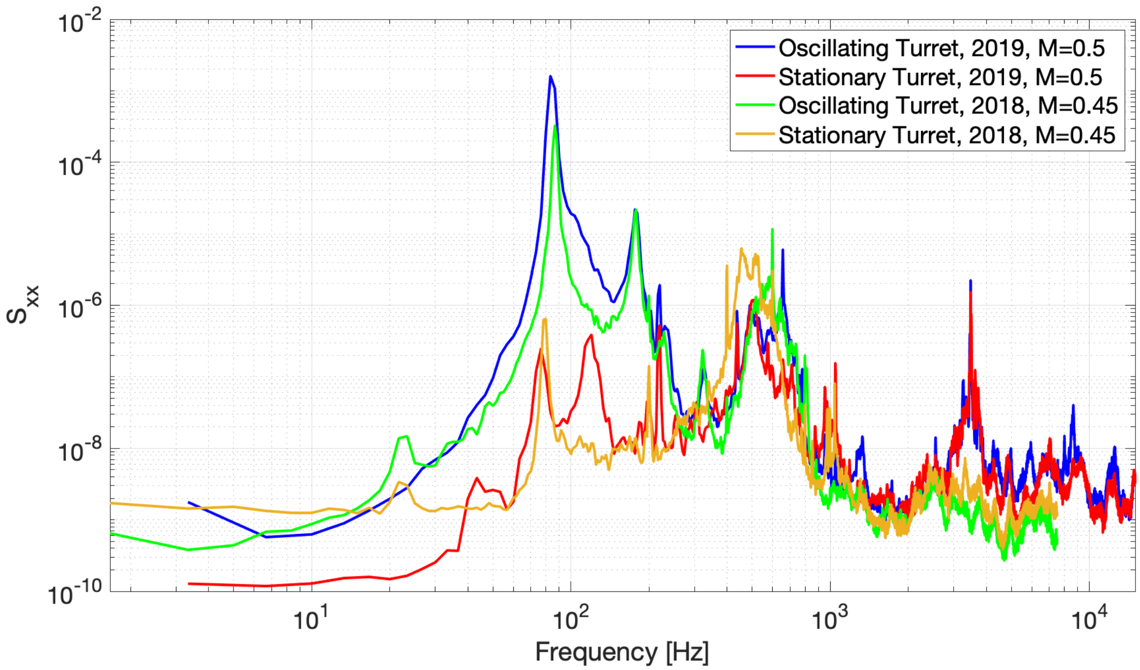

Figure 4: Amplitude spectra of the accelerometer spanwise turret motion for oscillating and stationary cases for both 2018 and 2019 tests.

To compensate for the tunnel blockage, the true freestream Mach number at the turret streamwise location in the test section, M_L, was estimated purely as a function of the cross-sectional area ratio, A_1/A_2 and the freestream Mach number, M, measured at the tunnel inlet, using equation (12)

$$f(M_L) = \left(\frac{A_1}{A_2}\right) f(M) \tag{12}$$

where the Mach number functions, $f(M)$ and $f(M_L)$, are given by equations (13) and (14), respectively. A_1 = 3 ft x 3 ft = 0.836 m^2 is the tunnel cross-section and $A_2 = A_1 - A_{turret}$, with the turret cross-section area, $A_{turret} = 0.5\pi R^2 = 0.025$ m^2, giving $A_1/A_2 = 1.031$.

$$f(M) = M\left[1 + \frac{\gamma - 1}{2} M^2\right]^{\frac{-(\gamma+1)}{2(\gamma-1)}} \tag{13}$$

$$f(M_L) = M_L\left[1 + \frac{\gamma - 1}{2} M_L^2\right]^{\frac{-(\gamma+1)}{2(\gamma-1)}} \tag{14}$$

Once the right side of equation (12) is obtained for a given M using the cross-sectional area ratio and equation (13), the resulting value is substituted into the left side of equation (14), and then equation (14) is solved for M_L. The blockage-corrected Mach numbers at the turret streamwise location corresponding to the freestream Mach numbers at the test section inlet are presented in

Table 2. The presence of the turret resulted in a maximum cross-sectional area reduction of only 3%. Consequently, the local freestream Mach numbers presented in Table 2, right, are higher than the values measured at the test section inlet presented in Table 2, left, by ~5%. These blockage-corrected freestream Mach numbers should be considered the true freestream Mach numbers for all results presented in these tests.

Table 2: Blockage-Corrected Freestream Mach Numbers at the Turret Streamwise Location

Test Section Inlet Mach Number, M	Blockage-Corrected Freestream Mach Number, M_L, from Eqn. (13)
0.40	0.42
0.50	0.52
0.60	0.63

Using the globally-reconstructed static pressure fields from PSP, p(x,y,t), the freestream Mach number, M, the far-field total pressure measured by the Pitot probe in the test section across from the turret, p_∞, and the compressible flow relation given by equation (15), the rms coefficient of pressure distributions, C_p, were computed for each Mach number and turret configuration in order to study the magnitude of fluctuations resulting from the unsteady pressure distribution on the turret and in the wake,

$$C_p = \frac{2}{\gamma M^2}\left(\frac{p(x,y,t)}{p_\infty} - 1\right) \tag{15}$$

The rms coefficient of pressure distributions for the oscillating and stationary cases at M = 0.4, 0.5, and 0.6 are presented in Figures 5, 6, and 7, respectively. There is a noticeable difference between the oscillating and stationary wake response as the oscillating turret appears to weaken the turbulent wake, as well as to extend its streamwise size. This effect also appears to become more prominent as the freestream Mach number increases.

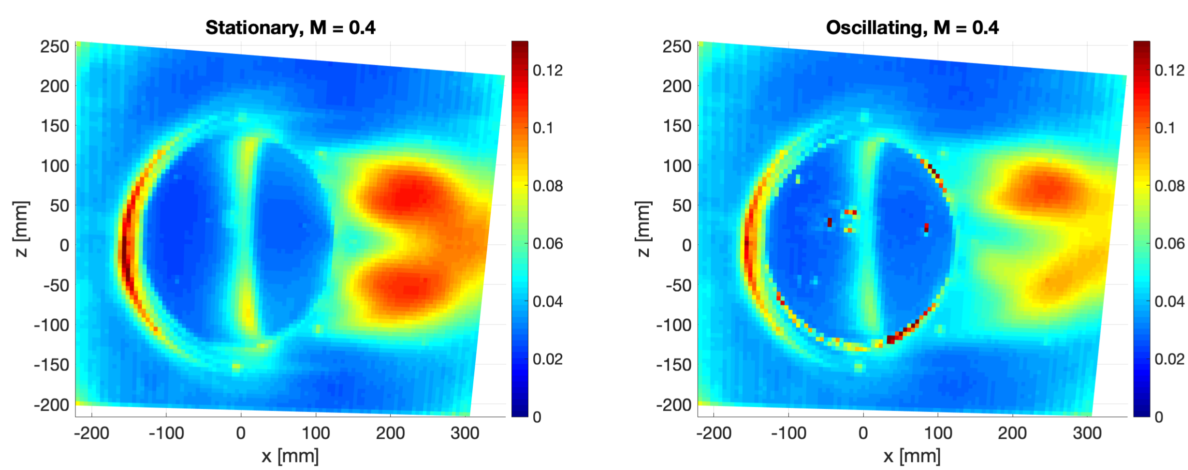

Figure 5: Normalized RMS coefficient of pressure distributions at M = 0.4 for the stationary turret, left, and the oscillating turret, right.

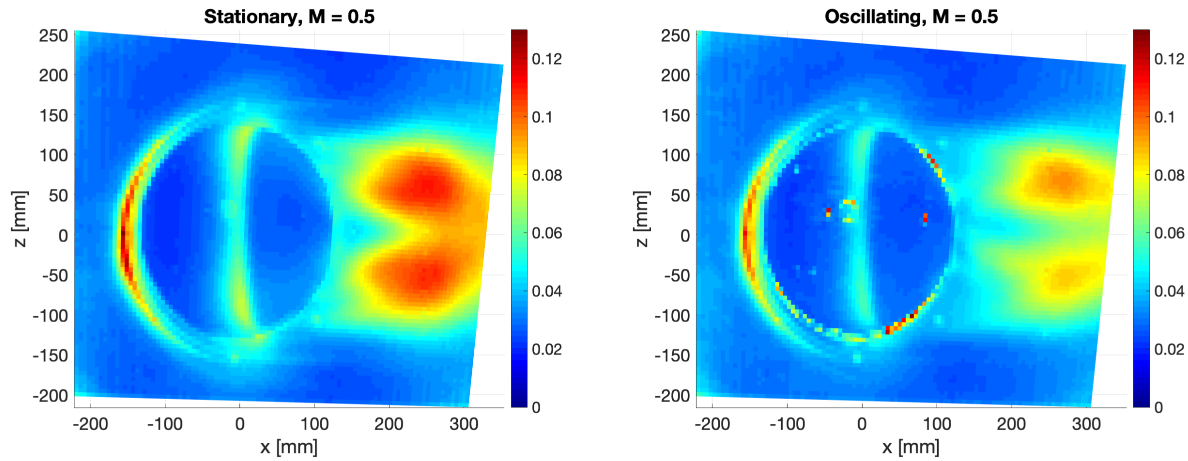

Figure 6: Normalized RMS coefficient of pressure distributions at M = 0.5 for the stationary turret, left, and the oscillating turret, right.

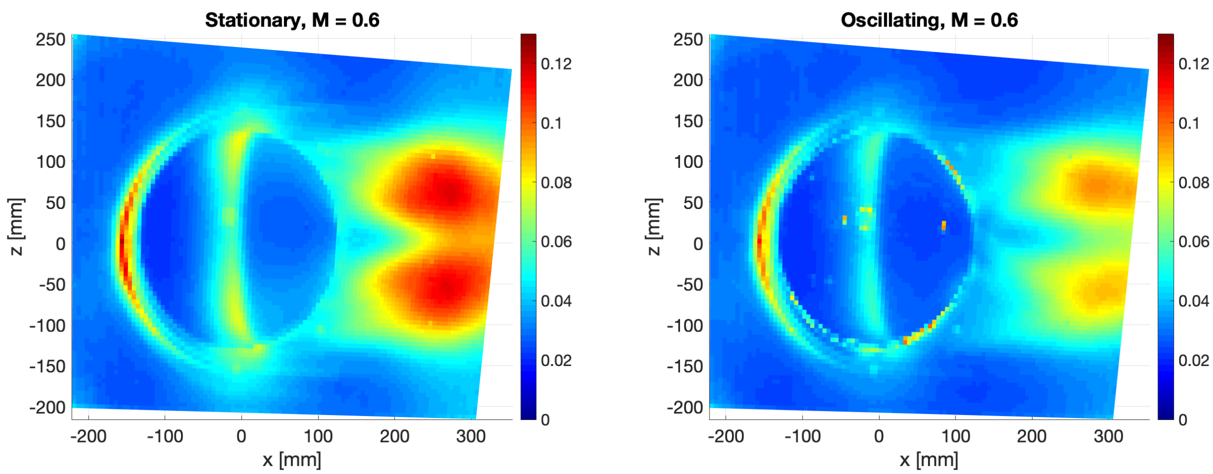

Figure 7: Normalized RMS coefficient of pressure distributions at M = 0.6 for the stationary turret, left, and the oscillating turret, right.

The first six JPOD spatial modes were computed for M = 0.5 and are presented in Figure 8. The first number in parenthesis in the title of each mode is the individual energy of that particular mode, and the second number in parenthesis is the cumulative energy of all modes prior to and including that particular mode. Overall, these modes contribute over 67 % of the unsteady pressure energy in the wake region. The first dominant mode is symmetric in the spanwise direction, while the second, the third mode, and the sixth mode are spanwise anti-symmetric for all Mach numbers. These modes were attributed to the presence of the global wake breathing and the wake shifting behavior, respectively, as discovered in [13,14].

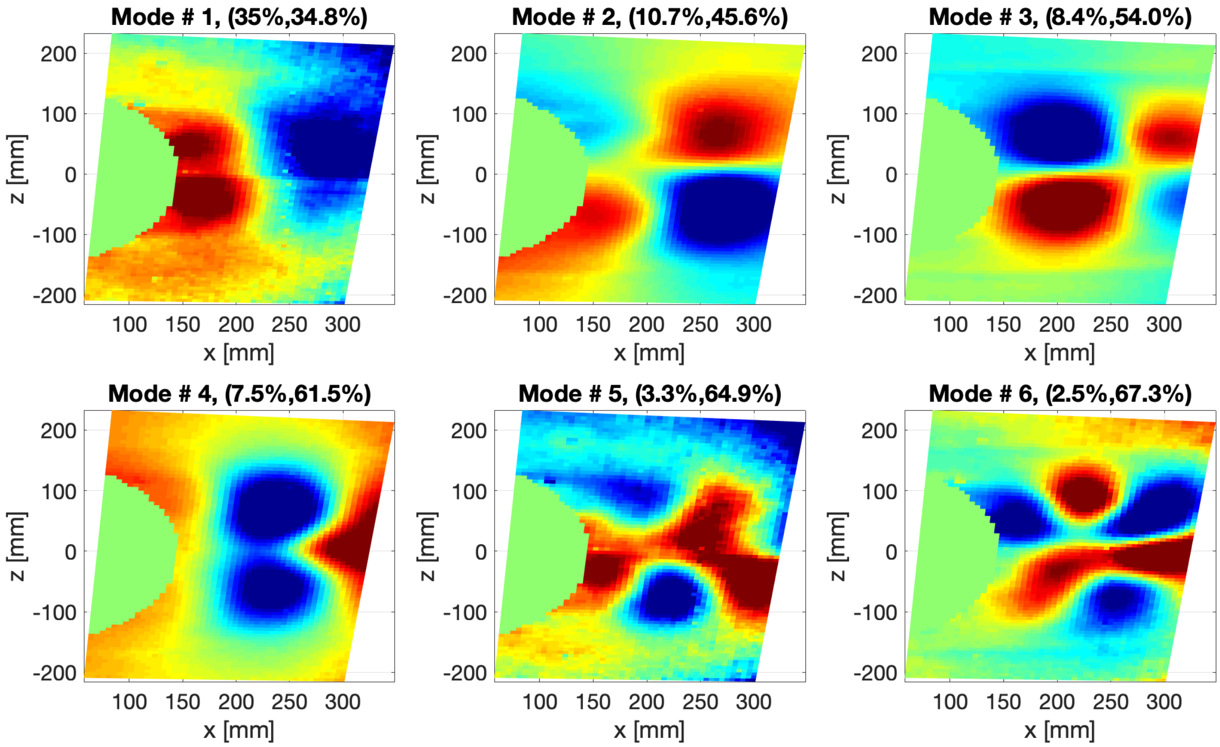

Figure 8: First six dominant JPOD spatial modes, which are common for both the stationary and the oscillating turret cases, at M = 0.5.

The corresponding spectra of the temporal coefficients for the stationary and oscillating cases at M = 0.5 is presented in Figure 9. The frequency was normalized by multiplying by the diameter of the turret and dividing by the freestream velocity, in order to be expressed in terms of Strouhal number, St_D. The dynamics of the spanwise symmetric mode, Mode #1, is mostly unchanged between the stationary and oscillating cases. The global wake shifting modes, represented by JPOD modes #2, #3, and #6, all have a distinct peak in their temporal coefficient spectra. The peaks are significantly suppressed for the oscillating case compared to the stationary case. The motion of the oscillating turret is driven by the unsteady turbulent flow. This behavior provides very strong evidence that the resulting mechanical motion of the turret driven by the unsteady turbulent flow reduces the overall energy of the wake, thus suppressing the wake dynamics at the frequency of the peaks.

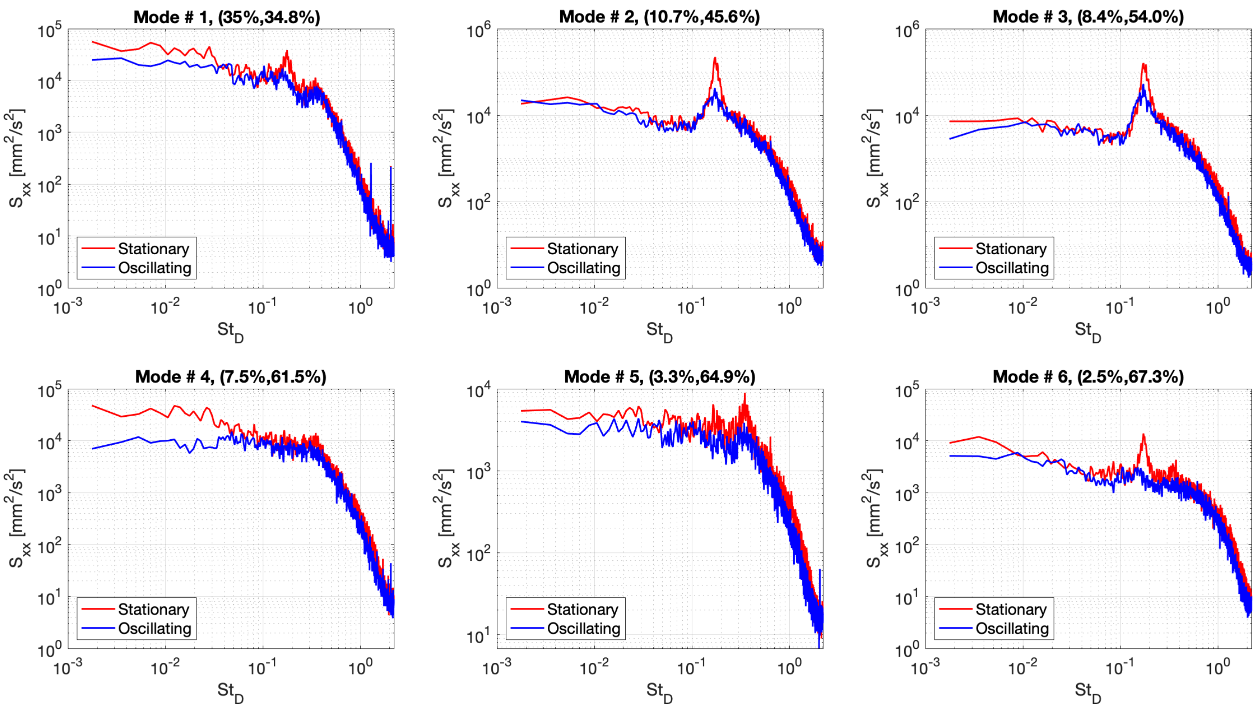

Figure 9: JPOD temporal coefficient spectra corresponding to the first six dominant JPOD modes, for the stationary and the oscillating turret cases at M = 0.5.

DMD was performed on the oscillating and stationary turret wake PSP pressure fields at M = 0.4, 0.5, and 0.6. The spectrum of the DMD amplitudes were used to identify the dominant frequencies at which the wake responded to the flow-induced turret oscillations generated by the unsteady pressure fields along with differences in the wake response between the oscillating and stationary cases, and to verify the behavior of JPOD temporal coefficient spectra. The spatial modes corresponding to the dominant frequencies in the DMD spectrum allow the spatial characteristics of the mode structures for each turret configuration to be studied and related to the wake shifting and breathing modes.

The normalized DMD spectra for the oscillating and stationary turret wake PSP pressure fields at M = 0.5 is presented in Figure 10. The spectra are simply the DMD energies given by the $|c_k|^2$ coefficients corresponding to each frequency. The stationary turret spectra generally contain higher energy levels compared to the oscillating turret spectra across the entire band of normalized frequencies. There are many sharp peaks in the spectra related to the wake shifting and breathing modal behavior, and the temporal resolution of the spectrum is quite high due to the considerably high sampling frequency over a relatively long sampling time.

There is also a broad peak in each spectrum corresponding to the dominant frequency response of the wake. Although not shown here, the dominant frequency of the wake response at M = 0.4 is f = 100 Hz, which corresponds to the normalized frequency St_D = 0.184. At M = 0.5, the dominant frequency increases to f = 119 Hz, resulted in the normalized frequency of St_D = 0.174, as shown in Figure 10. At M = 0.6, (not shown) the dominant frequency increases again to

141 Hz, corresponding to a normalized value of $St_D = 0.171$. The dominant frequency of the wake response matches the dominant wake response frequency presented in JPOD temporal coefficient spectra for all tested Mach numbers. The normalized resonant frequency of the oscillating turret itself was $St_D = 0.154$, 0.123, and 0.102 at M = 0.4, 0.5, and 0.6, respectively, yet the wake was found to consistently respond at a higher normalized frequency, $St_D \sim 0.17$, than the frequency of turret oscillations. Thus, the wake response is relatively independent of the Mach number, unlike the normalized frequency of the turret oscillations, which decrease with the increasing Mach numbers.

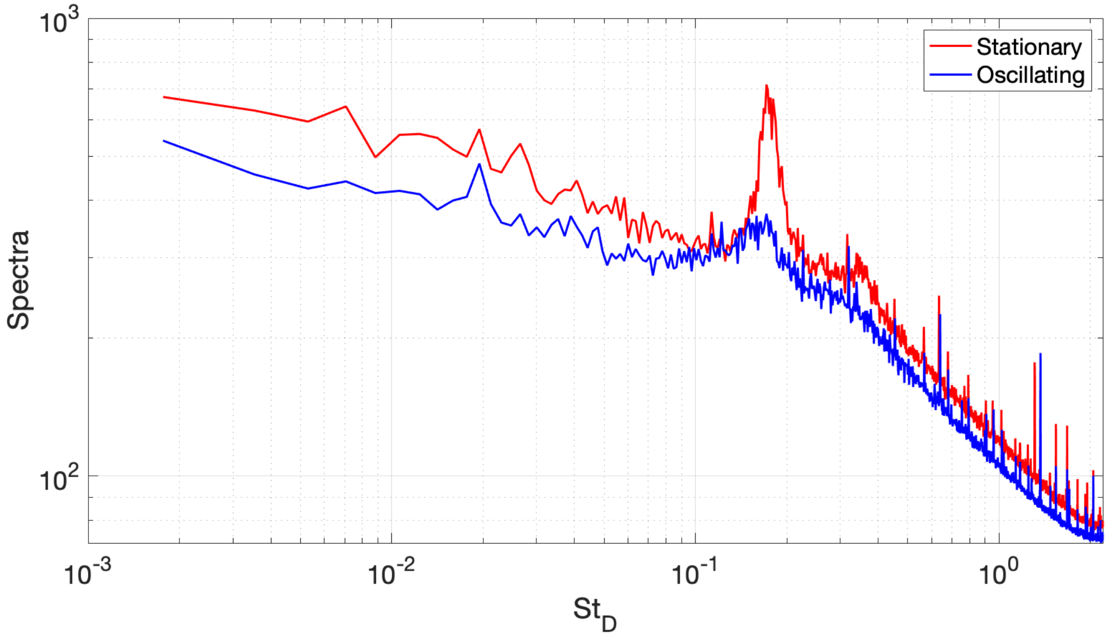

Figure 10: DMD spectra of the stationary and oscillating turret wake response at M = 0.5.

The DMD spatial modes corresponding to the dominant normalized frequencies of the wake response were computed for the stationary and oscillating configurations at all tested Mach numbers. The DMD spatial modes are presented for both configurations at M = 0.5, in Figure 11. The turret itself was masked with zeros in order to reduce contamination of the spectra and spatial modes so the surrounding wake region only could be studied. At M = 0.5, the DMD spatial modes of the stationary turret dominant wake response are clearly spanwise-antisymmetric. The antisymmetric mode was previously found to be related to the wake shifting behavior in [13]. The shifting mode is drastically suppressed for the oscillating case, where virtually all of the pressure energy in the wake has been extinguished, with only a slight indication of the antisymmetric mode visible when presented on the same scale. These findings confirm the results previously suggested from the DMD spectra along with JPOD temporal coefficient spectra corresponding to the antisymmetric modes.

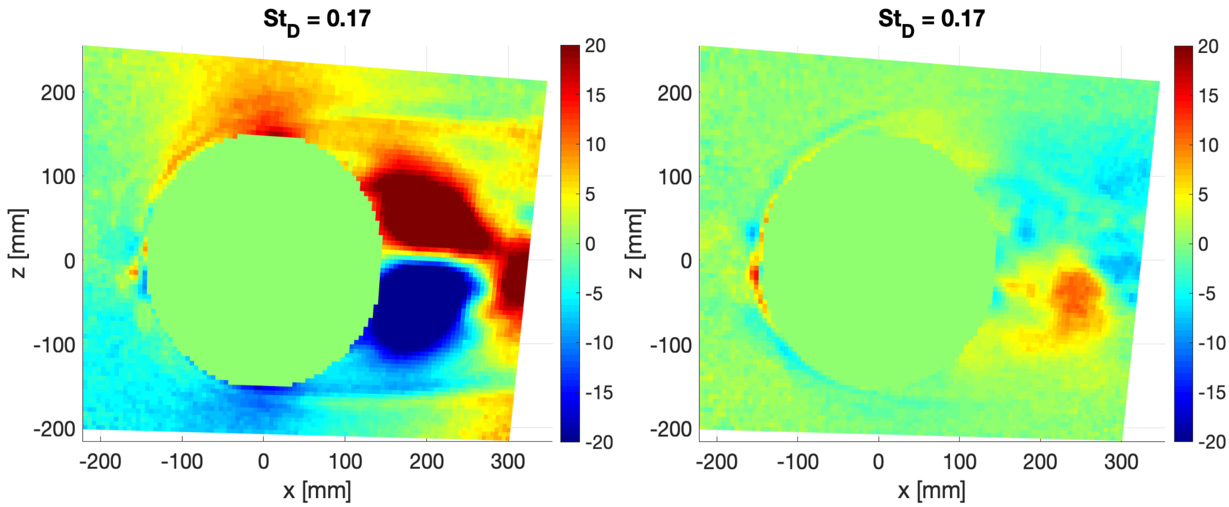

Figure 11: DMD spatial modes for the stationary turret, left, and the oscillating turret, right, at the dominant normalized wake response frequency for M = 0.5.

The consistent reduction in wake pressure energy is logical from an energy conservation standpoint. When the total energy of the flow, which remains constant throughout the control volume of the test section, is converted into work being done in order to move the turret back and forth in the spanwise direction, less energy is available in the wake to form convective structures and create shifting and breathing mode behavior that is readily observed for a fixed turret. This analysis provides useful information that will aid in developing a comprehensive fluid mechanical model of the flow downstream of a hemispherical spanwise-oscillating turret.

Although the primary focus of this work is on the wake response downstream of the spanwise-oscillating hemispherical turret, a comparison of the flow-induced unsteady forces on the turret itself for the stationary and oscillating cases is also relevant in understanding the full-field ramifications of changes in the wake on the aero-mechanical response of the turret. The representative time-averaged pressure fields mapped onto the oscillating and stationary turrets at M = 0.5 are presented in Figure 12.

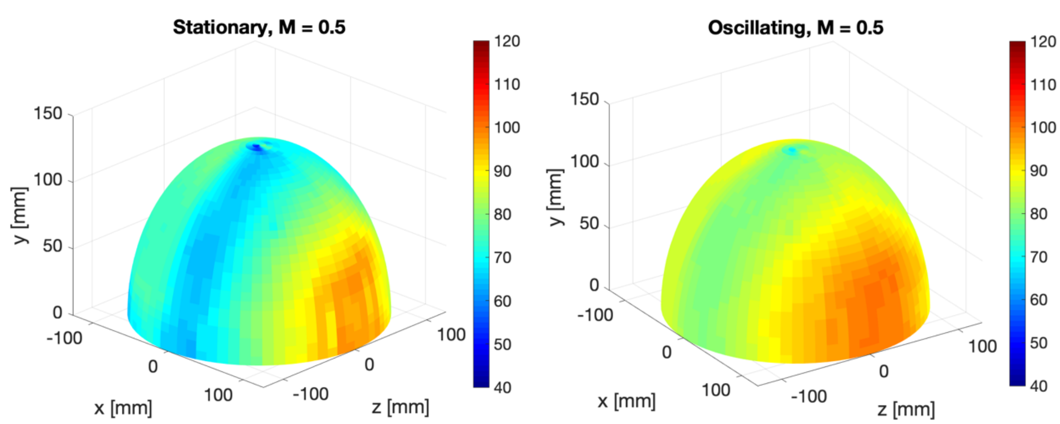

Figure 12: Time-averaged globally-reconstructed pressure fields for the stationary turret, left, and the oscillating turret, right, at M = 0.5.

The RMS forces on the oscillating and stationary turrets were normalized by the dynamic pressure for all tested Mach numbers, along with the cross-sectional area of the turret, *S*, yielding a non-dimensional quantity called coefficient of force, *C*, where the rms value, C_{rms}, is defined by equation (16).

$$C_{rms} = \frac{F_{RMS}}{0.5\rho_\infty U_\infty^2 S} \tag{16}$$

Table 3: Force Coefficients, C_{rms}

Configuration	M	$C_{x,rms}$	$C_{y,rms}$	$C_{z,rms}$
Stationary	0.40	0.0156	0.0364	0.0672
Oscillating	0.40	0.0160	0.0380	0.0632
Stationary	0.50	0.0168	0.0476	0.0672
Hemisphere-on-cylinder, from [16]	0.50	0.031	0.022	0.053
Oscillating	0.50	0.0108	0.0252	0.0420
Stationary	0.60	0.0184	0.0572	0.0772
Oscillating	0.60	0.0172	0.0476	0.0528

The coefficients of force are presented in Table 3 for the oscillating and stationary turrets at M = 0.4, 0.5, and 0.6. As expected, the highest magnitude of fluctuating force on the turret occurs in the spanwise z-direction for both cases. The coefficient of force is over 50% higher in the z-direction than in the wall-normal y-direction and between three and four times higher in the streamwise x-direction for both turret configurations at all three Mach numbers. The coefficients of force computed for the stationary turret agree reasonably well with the values found by De Lucca, et al. in extensive hemisphere-on-cylinder turret studies conducted in wind tunnels and in-flight, as presented in [16,20]. The different diameter of the hemisphere-on-cylinder turret used in these studies, 12 in., is accounted in the normalized value of the unsteady force, since it is divided by the cross-sectional area, including the cylindrical portion of the turret. However, the presence of the cylinder would move the hemispherical part of the turret away from the time-varying necklace vortex, thus reducing the pressure field on both sides of the hemisphere. Since the purely hemispherical oscillating turret in this study sits directly on the tunnel wall, the necklace vortex would contribute additional pressure and unsteady force fluctuations in the spanwise direction, and this is reflected in the higher $C_{z,rms}$ values in Table 3 compared to the other two directions. Also, the reliability of the pressure measurements at the front and at the back of the turret is limited due to the orientations of the cameras. These regions contribute the most to the streamwise force, or drag, so the values presented in Table 3 are likely an underestimate of the true values.

Spectra of the x, y, and z-components of the unsteady forces on the oscillating and stationary turrets are presented as a function of Strouhal number at M = 0.5 in Figure 13. A distinct peak is present in the *z*-component of the oscillating turret unsteady force spectra, which corresponds to the 84 Hz resonant frequency of the oscillating turret. This was found to be the case for all Mach numbers tested. There is also a sharp peak in the *z*-component of the stationary turret spectra, and the normalized frequency of this peak matches the frequency of the shifting mode discovered from JPOD and DMD analysis. A broad peak with lower energy is noticeable in the oscillating turret force spectra at the normalized frequency of the sharp peak in the stationary turret force spectra, and it appears to be significantly dampened with respect to the stationary case. This behavior was also ubiquitous for all Mach numbers tested. These findings indicate that the wake shifting mode creates unsteady forces on the stationary turret, and the modification of the wake shifting mode from flow-induced turret oscillations suppresses the unsteady forcing on the turret from the shifting mode in addition to the wake dynamics.

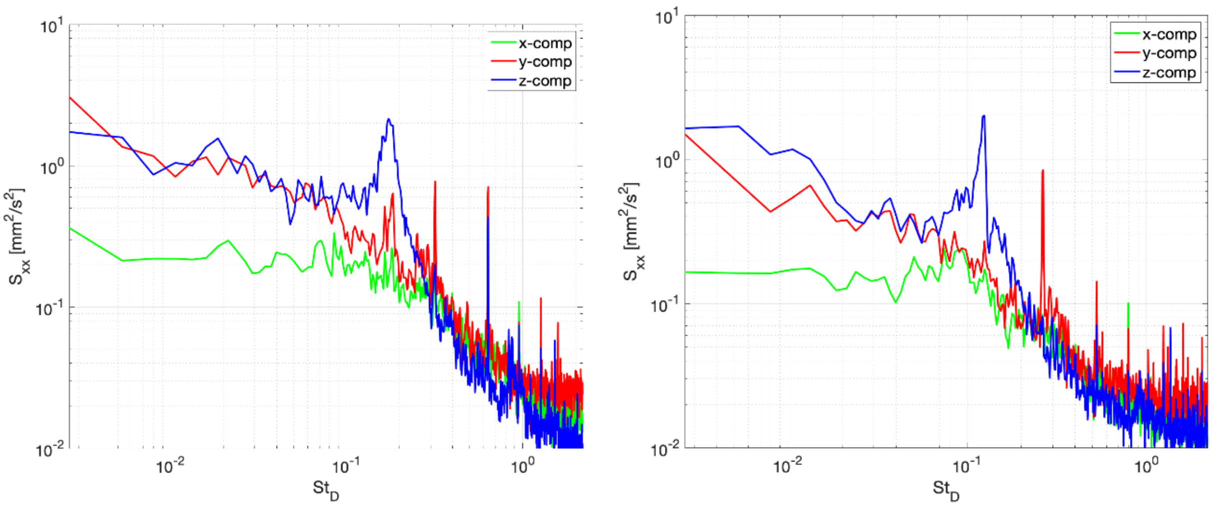

Figure 13: *x*, *y*, and *z*-components of unsteady force spectra for the stationary turret, left, and the oscillating turret, right, at M = 0.5.

V. Conclusions

An extensive study using pressure-sensitive paint (PSP) was then conducted in order to investigate the globally-reconstructed pressure fields on and around both oscillating and stationary turrets. The coefficient of pressure distributions in the wake indicated that flow-induced turret oscillations suppress the total pressure energy at all three tested Mach numbers, M = 0.4, 0.5, and 0.6. JPOD and DMD modal analysis techniques were applied in order to investigate the frequency response of the wake dynamics for the oscillating and stationary cases. The first six JPOD spatial modes were found to constitute over 65% of the unsteady pressure energy in the wake at M = 0.4 and 0.5, and over 70% at M = 0.6. JPOD temporal coefficient spectra revealed a sharp peak at $St_D \sim 0.17$, which corresponded to the wake shifting mode, and this peak was substantially suppressed for the oscillating case at all three Mach numbers. The first five cumulative and individual mode energies were also found to be higher for the stationary case compared to the oscillating case. Therefore, the resulting mechanical motion of the turret was found to reduce the overall energy of the wake, thus suppressing the wake dynamics at the frequency of the wake shifting mode.

DMD analysis of the wake unsteady PSP pressure fields verified the results obtained from JPOD, where spectra of the DMD mode coefficients revealed the wake response of the stationary turret to occur at the normalized frequency $St_D \sim 0.17$. DMD spectra of the oscillating turret wake contained lower levels of energy across the entire band of sampling frequencies. DMD spatial modes presented for both stationary and oscillating cases at this frequency also revealed the shifting mode to be the primary feature of the stationary turret wake response and confirmed that the shifting mode is substantially suppressed when the flow induces single-frequency motion of the turret near this frequency in the spanwise direction. An unsteady force analysis of the turret itself found that most of the unsteady forcing for both turret configurations occurs in the spanwise direction, and unsteady force spectra revealed that the dominant frequency corresponded to the resonant oscillating frequency for the oscillating turret and the dominant wake response frequency for the stationary turret. The results are logically interpreted in the context of energy conservation, where the energy in the wake must be reduced in order for the flow to do work on the oscillating turret.

Acknowledgements

This work is supported by the Air Force Research Laboratory, Cooperative Agreement number FA9451-17-2-0088. The U.S. Government is authorized to reproduce and distribute reprints for governmental purposes notwithstanding any copyright notation thereon.

References

[1] S. Gordeyev and E. Jumper, "Fluid Dynamics and Aero-Optics of Turrets", Progress in Aerospace Sciences, 46, (2010), pp. 388-400.

[2] B. Vukasinovic, A. Glezer, S Gordeyev, E. Jumper and W. W. Bower, "Flow Control for Aero-Optics Application", Experiments in Fluids, 54, p. 1492, 2013.

[3] N. De Lucca, S. Gordeyev and E.J. Jumper, "In-flight aero-optics of turrets", Journal of Optical Engineering, 52(7), 071405, 2013.

[4] C. Porter, S. Gordeyev, M. Zenk and E. Jumper, "Flight Measurements of the Aero-Optical Environment around a Flat-Windowed Turret", AIAA Journal, Vol. 51, No. 6, Jun. 2013, pp. 1394-1403.

[5] J. Morrida, S. Gordeyev, N. De Lucca, E.J. Jumper, " Shock-Related Effects on Aero-Optical Environment for Hemisphere-On-Cylinder Turrets at Transonic Speeds ", Applied Optics, 56(16), pp. 4814-4824, 2017.

[6] E. Mathews, K. Wang, M. Wang and E. Jumper, "LES of an Aero-Optical Turret Flow at High Reynolds Number", AIAA 2016-1461, 2016.

[7] R. Jelic, S. Sherer and R.Greendyke, "Simulation of Various Turret Configurations at Subsonic and Transonic Flight Conditions Using OVERFLOW", Journal of Aircraft, 50, pp. 398-409, 2013.

[8] Coirier, W.J, Porter, C., Barber, J., Stutts, J., Whiteley, M., Goorskey, D. and Drye, R.," Aero-Optical Evaluation of Notional Turrets in Subsonic, Transonic and Supersonic Regimes," AIAA Paper 2014-2355, 2014.

[9] Evaluation of Notional Turrets in Subsonic, Transonic and Supersonic Regimes," AIAA Paper 2014-2355, 2014

[10] P.E. Morgan and M.R. Visbal, "Hybrid Reynolds-Averaged Navier–Stokes/Large-Eddy Simulation Investigating Control of Flow over a Turret," Journal of Aircraft, Vol. 49, No. 6, pp. 1700-1717, 2012.

[11] Ladd, J., Mani, A. and Bower, W., “Validation of Aerodynamic and Optical Computations for the Unsteady Flow Field About a Hemisphere-on-Cylinder Turret,” AIAA Paper 2009-4118, 2009.

[12] S. Gordeyev, N. De Lucca, E. Jumper, K. Hird, T.J. Juliano, J.W. Gregory, J. Thordahl and D.J. Wittich, " Comparison of Unsteady Pressure Fields on Turrets with Different Surface Features using Pressure Sensitive Paint ", Experiments in Fluids, 55, p. 1661, 2014.

[13] S. Gordeyev, N. De Lucca, J. Morrida, E.J. Jumper, and D.J. Wittich, " Conditional Studies of the Wake Dynamics of Hemispherical Turret Using PSP ", AIAA Paper 2018-2048, 2018.

[14] N. De Lucca, S. Gordeyev, J. Morrida, E.J. Jumper, and D.J. Wittich, " Modal Analysis of the Surface Pressure Field Around a Hemispherical Turret using Pressure Sensitive Paint ", AIAA Paper 2018-0932, 2018.

[15] S. Gordeyev, N. De Lucca, J. Morrida, E.J. Jumper, and D.J. Wittich, " Conditional Studies of the Wake Dynamics of Hemispherical Turret Using PSP ", AIAA Paper 2018-2048, 2018.

[16] N. De Lucca, S. Gordeyev, E. Jumper, K. Hird, T.J. Juliano, J.W. Gregory, J. Thordahl and D.J. Wittich, " The Estimation of the Unsteady Aerodynamic Force Applied to a Turret in Flight ", AIAA Paper 2013-3136, 2013.

[17] A Roeder, S. Gordeyev, and D.J. Wittich, “Wake Response Downstream of Spanwise-Oscillating Hemispherical Turret”, AIAA Paper 2020-0685, 2020.

[18] A. Erturk and D.J. Inman, *Piezoelectric Energy Harvesting*, 1st Edition, John Wiley & Sons, Ltd, 2011.

[19] K. Taira, S.L. Brunton, S.T.M. Dawson, C.W. Rowley, T. Colonius, B.J. McKeon, O.T. Schmidt, S. Gordeyev, V. Theofilis, L.S. Ukeiley, "Modal Analysis of Fluid Flows: An Overview", *AIAA Journal*, Vol. 55(12), pp. 4013-4041, 2017.

[20] N. De Lucca, 2015, Studies of the Pressure Field and Related Beam Jitter for Hemisphere-on-Cylinder Turrets, PhD thesis, University of Notre Dame.

[21] Chen, K. K., Tu, J. H., and Rowley, C.W., “Variants of Dynamic Mode Decomposition: Boundary Condition, Koopman, and Fourier Analyses,” Journal of Nonlinear Science, Vol. 22, No. 6, pp. 887–915, 2012.